Atomic-resolution STM of a system with strongly correlated electrons: NiO(001) surface structure and defect sites

M. R. Castell

Department of Materials, University of Oxford, Parks Road, Oxford OX1 3PH, United Kingdom

P. L. Wincott

IRC in Surface Science and Chemistry Department, Manchester University, Manchester M13 9PL, United Kingdom

N. G. Condon

IRC in Surface Science, University of Liverpool, Liverpool L69 3BX, United Kingdom

C. Muggelberg

Department of Materials, University of Oxford, Parks Road, Oxford OX1 3PH, United Kingdom

G. Thornton

IRC in Surface Science and Chemistry Department, Manchester University, Manchester M13 9PL, United Kingdom

S. L. Dudarev, A. P. Sutton, and G. A. D. Briggs

Department of Materials, University of Oxford, Parks Road, Oxford OX1 3PH, United Kingdom

Elevated-temperature scanning tunneling microscopy has been used to obtain atomic resolution images of (001) surfaces of NiO single crystals. Empty-state images of the (1×1) surface show the nickel-atom sites and filled-state images show the oxygen ions in agreement with recent theoretical studies of the electronic structure of NiO. Empty-state and filled-state images of point defects and patterning effects observed on the upper terraces of $\langle 100 \rangle$ step edges are explained by directional $2p$-$3d$ covalent bonding between the oxygen and nickel sublattices. [S0163-1829(97)02311-4]

I. INTRODUCTION

Recent developments in the theoretical understanding of the electronic structure of transition-metal compounds[1-5] (TMC's) have confirmed Mott's idea[6] that the origin of band gaps in these materials is associated with strong on-site repulsion between electrons in the localized d states of the metal ions. Depending on the relative position of the metal d levels and the oxygen p levels on the energy scale, and on the magnitude of the Hubbard U characterizing the on-site Coulomb electron-electron interaction, transition metal oxides can be classified into two types. If the upper edge of the valence band is predominantly of d or p character then the oxide is a Mott-Hubbard or charge-transfer insulator, respectively.[2] According to this classification, results of calculations of the electronic structure of NiO suggest that it is a charge-transfer insulator with strongly correlated electrons.[3-5]

Progress in the understanding the electronic structure of TMC's has been largely due to the development of experimental techniques. Results from core x-ray photoemission spectroscopy (XPS) and bremsstrahlung isochromat spectroscopy[1,7,8] (BIS) have stimulated attempts to analyze these data using either the configuration-interaction (CI) approach[9] or the Anderson impurity model.[2] This methodology has proved to be more informative than earlier studies of the transport properties of TMC's,[10] which were known to be strongly influenced by the presence of defects and by the details of quasiparticle interactions.

In this paper we argue that the potential of experimental techniques applied to the study of the transport properties of strongly correlated electronic systems such as TMC's is far from being exhausted, and we show that a substantial amount of information inaccessible to XPS and BIS can be obtained from the analysis of scanning tunneling microscope (STM) images of these materials. The spatial resolution that can be achieved using a STM exceeds by orders of magnitude that of XPS and BIS, allowing real-space observations of the electronic structure of perfect and defective surfaces. In this paper we present and analyze atomic resolution images of NiO surfaces containing flat areas and defects and propose a simple model explaining the origin of contrast patterns observed at step edges and around defect sites.

NiO crystals adopt the rocksalt structure with a lattice parameter $a_0 = 4.17$ Å. Cleavage on (001) planes is easily achieved and this results in a relatively flat and defect free surface. Low-energy electron diffraction (LEED) I-V studies on the UHV-cleaved surface have shown no detectable rumpling and revealed that the outermost ion plane relaxes inwards by $\sim 2\%$.[11,12] Calculations[13] also suggest that rumpling values are very low and that one can therefore regard the geometry of the (001) face as a near perfect bulk termination. STM studies of NiO crystals have not been reported, but some researchers[14] have investigated thin NiO films grown on metal crystal substrates.

In a purely ionic picture of NiO the Ni^{2+} ions have a partially filled d shell in a $3d^8$ ground-state configuration. According to conventional band theory the partially filled $3d$ e_g bands should result in metallic behavior,[15] but in fact due to strong on-site d-d electron-electron repulsion NiO
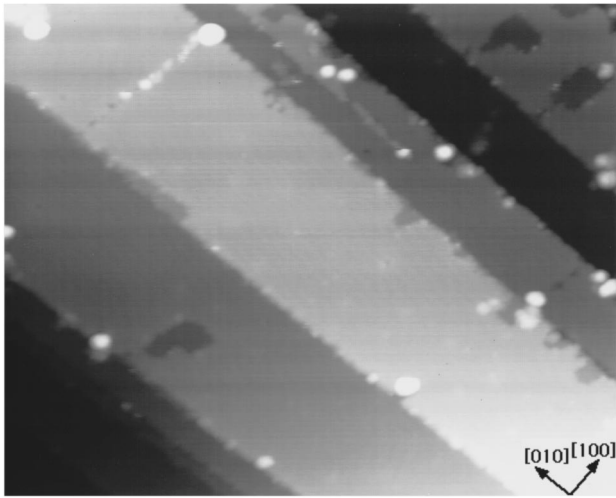
FIG. 1. Topography of the NiO cleavage surface showing large (001) terraces and monoatomic $\langle 010 \rangle$ steps. The STM image is 120 $\times 95$ nm^2 and was taken at $+3.5$ V sample bias, 1.0 nA tunneling current.

FIG. 2. Empty-state image ($+0.7$ V sample bias, 1.0 nA tunneling current) of the (1×1) terrace termination showing the Ni-ion sites and a bright adsorbate. The schematic inset indicates the atomic arrangement of the (001) surface where the Ni ions are bright and the O ions are small and dark. Only the Ni ions can be seen in the STM image.

becomes an insulator with a 4.3-eV bulk band gap.[1] Interpretation of the density of states spectra has proved very challenging[2–4,16]. The current picture is that the Ni $3d$ and O $2p$ states are hybridized, giving a large degree of mixing between these states in the valence band. The conduction band spectra are dominated by Ni $3d$ states.[2–4] Recent CI calculations[17] and electron-energy-loss spectroscopy (EELS) studies[18] indicate the existence of an empty surface state on the NiO (001) surface at 0.6 eV above the valence-band edge, which originates from Ni d states.

II. EXPERIMENTAL PROCEDURES

NiO crystals were grown from analar materials (impurity content below 10 ppm) by K & R Creations, Japan. Imaging experiments were carried out in a JEOL JSTM-4500XT elevated temperature UHV STM. NiO (001) faces were obtained through room temperature (RT) cleavage in the UHV chamber that has a base pressure of 2×10^{-8} Pa. The NiO crystals were heated radiatively by a tungsten filament next to the sample and independent temperature calibration resulted in an estimate of ~ 200 °C during the STM experiments. This heating resulted in an order of magnitude decrease in resistivity from ~ 100 Ω cm at RT. STM imaging was attempted at RT, but was not successful. Imaging was performed using etched polycrystalline tungsten tips. A four-grid VG Microtech rear view LEED/Auger electron spectroscopy system was used to determine the long-range order, crystal orientation, and cleanliness of the (001) cleavage surfaces. The results showed only very sharp (1×1) spots consistent with earlier work[11,12,19] and levels of contamination below the spectrometer detection limit.

III. RESULTS AND DISCUSSION

Figure 1 shows a STM image of the typical mesoscopic topography that is generated by cleavage. Relatively large (001) terraces can be seen that are separated by monoatomic steps that run predominantly in $\langle 010 \rangle$ directions. Step struc-

tures that lie at right angles to those in Fig. 1 were observed in other regions of the sample. Bright areas in this image are due to regions where contamination has accumulated. The terraces generally have a low defect density and are arranged in the bulk terminated (1×1) structure shown in the schematic inset in Fig. 2.
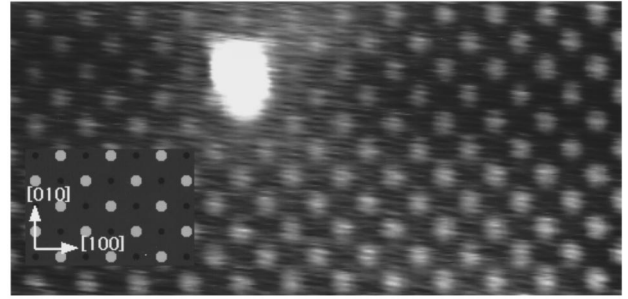
An empty-states image of such a region obtained at $+0.7$ eV sample bias is shown in Fig. 2. We interpret this image as resulting from tunneling into the unoccupied surface states found on this surface by EELS (Ref. 18) and CI calculations.[17] Since this state is localized on Ni sites we interpret the lattice seen in Fig. 2 as being the Ni sublattice. However, we cannot at this stage rule out the possibility that the lattice seen in Fig. 2 is the oxygen sublattice because of the finite covalent mixing between Ni d and O p states and because O p states probably extend further into the vacuum. Further support of our interpretation of Fig. 2 as an image of the Ni sublattice is provided by images of point defects, which we discuss in the next paragraph. Throughout our extensive STM study numerous empty states atomic resolution images were obtained of similar quality to that shown in Fig. 2. However, it should be stressed that acquiring these images was not routine and involved operating at low sample biases that frequently resulted in tip crashes. Filled-states atomic resolution images were obtained less often than empty-states images and also show (1×1) periodicity but in many cases the atomic corrugations are barely distinguishable above the noise level [see Fig. 3(b)]. Due to these experimental difficulties it was not possible to obtain filled and empty state images of identical regions of the surface.

Typical empty- and filled-states images of isolated point defects, which are occasionally observed on the terraces, are shown in Fig. 3. We were unable to obtain filled- and empty-states images from the same region of the sample, but Figs. 3(a) and 3(b) are typical of many observations of the same defect contrast patterns seen in empty and filled states. We will argue that the point defects shown in Figs. 3(a) and 3(b) are both located on the Ni sublattice.

Figure 4(a) shows the bulk density of states for antiferromagnetic NiO calculated using a linear muffin-tin orbital version of the local density approximation including the Hubbard U term with $U=8$ eV.[3,20] It is clear that there is substantial coupling between O p and Ni d states in the valence band. This implies that covalent bonding in NiO is
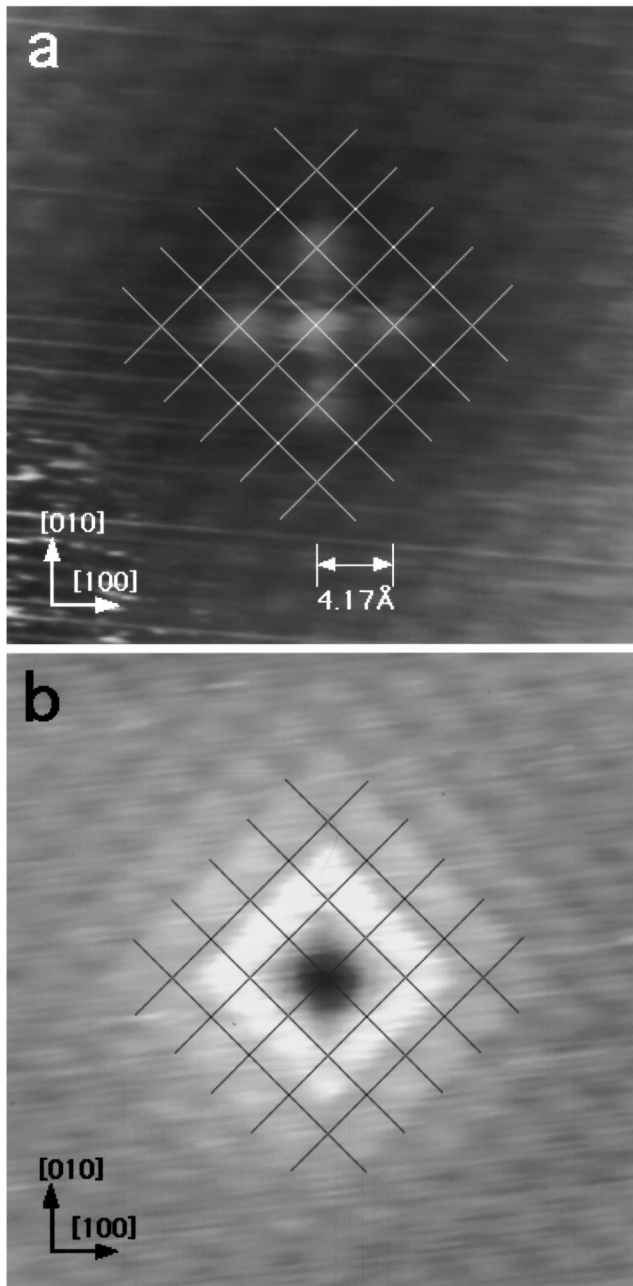
FIG. 3. (a) Empty-states (+1.2 V sample bias, 1.0 nA tunneling current) and (b) filled-states (−1.3 V sample bias, 1.0 nA tunneling current) STM images of a single point defect. In (a) the defect appears bright and is surrounded by four bright SNN Ni sites that are in registry with the Ni (1×1) sublattice (indicated by the overlaid mesh). In (b) the defect center again lies on the overlaid mesh, which is identical to that shown in (a). The bright spots seen away from the defect are therefore on the oxygen sublattice.

FIG. 4. (a) Calculated density of bulk states of antiferromagnetic NiO. (b) Schematic representation of covalent $2p$-$3d$ bonding between Ni and O ions on the (001) surface of NiO and defects at Ni and O sites.

almost entirely due to overlap between oxygen $2p$ states and nickel $3d$ states. d-d overlap between nearest-neighbor (NN) Ni ions is about 5 times weaker.[21] Therefore, to a first approximation, the d-d hopping may be ignored. A schematic diagram illustrating the real-space geometry of covalent bonding between oxygen p states and nickel d states is shown in Fig. 4(b). Since the p states on each oxygen ion are orthogonal, the two simple cubic sublattices, shaded dark and light gray in Fig. 4(b), are electronically decoupled in

the sense that an electron cannot hop between them. It follows that Ni ions are electronically coupled along the $\langle 100 \rangle$ directions through d-p hopping via intermediate oxygen ions, a picture that is consistent with Anderson's theory of superexchange.[22] Therefore, second-nearest-neighbor (SNN) Ni ions are effectively more strongly coupled than NN Ni ions.

Assume the defect is located on the O sublattice [see Fig. 4(b), left]. The NN oxygen sites are coupled to the defect through fourfold symmetric $d_{x^2-y^2}$ states on NN nickel sites. There are *two* paths by which an electron can hop between NN oxygen sites in the surface. Each path consists of two hops via a NN Ni site. But there is only *one* path of length two hops between SNN oxygen sites in the surface. Therefore, if the defect is located on the oxygen sublattice we expect the four NN oxygen sites to show a stronger contrast effect than the four SNN sites.

Assume now that the defect is located on the Ni sublattice [see Fig. 4(b), right]. We have already seen that NN Ni sites are electronically decoupled. However, SNN Ni sites are coupled by a single path of length two hops via intermediate oxygen p states. Therefore, if the defect is located on the
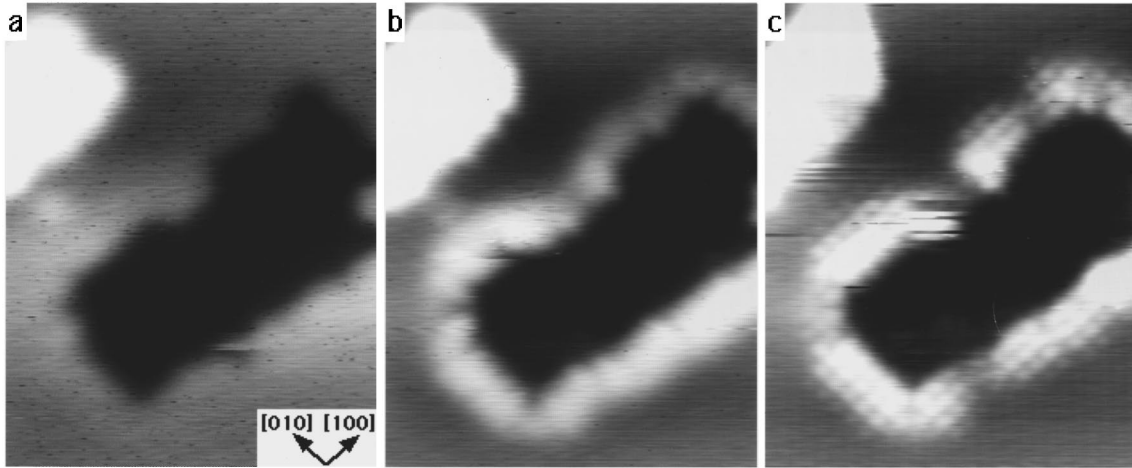
FIG. 5. Empty-states STM images (9×11 nm^2) of terraces separated by monoatomic steps taken at sample biases of (a) +3.5 V, (b) +2.5 V, (c) +0.7 V, and 1.0 nA tunneling currents. As the sample bias is lowered the mainly topographic contrast in (a) is affected by the presence of local electronic perturbations on the upper part of step edges (b) which manifests itself as a local brightening in the image. At low voltages (c) the brightening is resolved into $c(2 \times 2)$ patterning, but this occurs only above $\langle 100 \rangle$ step edges, not $\langle 110 \rangle$ step edges, which are also present in the image.

nickel sublattice we expect the four SNN Ni sites to show a stronger contrast effect than the four NN Ni sites.

The key difference between the expected contrast patterns is the separation s between the defect center and the nearest sites showing altered contrast. For a Ni-site defect s should be 4.17 Å, and for an O-site defect s should be 2.95 Å. It is clear from Fig. 3(a) that s is 4.17 Å and therefore the defect is located on a Ni site. Since this site is also located on the lattice that is imaged away from the defect we conclude that it is the Ni sublattice that is imaged in Figs. 2 and 3(a).

Consider Fig. 3(b). The size and orientation of the region around the defect showing strong contrast are the same as in Fig. 3(a). If the defect center were located on the oxygen sublattice we would expect the contrast pattern to be rotated by 45° and the size to be $1/\sqrt{2}$ smaller. The mesh in Fig. 3(b) is identical to that in Fig. 3(a), and it passes through the defect center. The four NN sites to the defect center on the same sublattice show slightly weaker contrast than the four SNN sites. This is inconsistent with the defect center being located on the oxygen sublattice. We again conclude that the defect is located on the Ni sublattice. The fact that the mesh is located *between* rows of brighter sites seen away from the defect indicates that the perfect lattice of brighter sites seen in filled-states images is the *oxygen* sublattice. This inference and the smaller corrugations seen in Fig. 3(b) than in Fig. 3(a) are consistent with a large contribution to the valence-band states from both sublattices, as seen in Fig. 4, and a greater extension of oxygen p_z states into the vacuum than nickel $d_{3z^2-r^2}$ states.

The overall darkening in Fig. 3(a) and brightening in Fig. 3(b) around the defect center indicate that both defects are negatively charged. Since both defects also lie on the Ni sublattice it is probable that they are the same type of defect, e.g., a Ni vacancy.

The brightening of the SNN Ni ions shown in Fig. 3(a) displays $c(2 \times 2)$ symmetry. This patterning can also be observed at the top of $\langle 100 \rangle$ step edges. Figure 5 shows a variable bias series of empty-states images. In Fig. 5(a) the gross terrace structure can be identified. When the sample bias is lowered in Fig. 5(b) the top of the $\langle 100 \rangle$ terrace steps is highlighted. In Fig. 5(c), taken at even lower voltage, a $c(2 \times 2)$ pattern is resolved, resembling that of Fig. 3(a). These images can be interpreted following the same arguments as those above. Bright rows of Ni sites parallel to the $\langle 100 \rangle$ step edges may be seen. The row spacing of 4.17 Å indicates that every *second* Ni site is highlighted, as in Fig. 3(a). But this pattern is absent along the $\langle 110 \rangle$ step edges. These features are entirely consistent with strong p-d coupling along $\langle 100 \rangle$ and its absence along $\langle 110 \rangle$ directions, as shown in Fig. 4.

IV. CONCLUSION

We have reported atomic resolution STM observations of the (001) surface of NiO single crystals obtained at elevated temperature. The nickel sites are seen in empty-states images and the oxygen sites are seen in filled-states images. These results provide experimental evidence that NiO is a charge-transfer insulator with strongly correlated electrons and not a Mott-Hubbard insulator.

ACKNOWLEDGMENTS

[1] G. A. Sawatzky and J. W. Allen, Phys. Rev. Lett. **53**, 2339 (1984).

[2] J. Zaanen, G. A. Sawatzky, and J. W. Allen, Phys. Rev. Lett. **55**, 418 (1985); J. Zaanen and G. A. Sawatzky, Prog. Theor. Phys. Suppl. **101**, 231 (1990).

[3] V. I. Anisimov *et al.*, Phys. Rev. B **44**, 943 (1991); **48**, 16 929 (1993).

[4] M. Arai and T. Fujiwara, Phys. Rev. B **51**, 1477 (1995).

[5] F. Aryasetiawan and O. Gunnarsson, Phys. Rev. Lett. **74**, 3221 (1995).

[6] N. F. Mott, *Metal-Insulator Transitions* (Taylor & Francis, London, 1974).

[7] Z.-X. Shen *et al.*, Phys. Rev. Lett. **64**, 2442 (1990).

[8] S. Hüfner, Adv. Phys. **43**, 183 (1994).

[9] A. Fujimori, F. Minami, and S. Sugano, Phys. Rev. B **29**, 5225 (1984); **30**, 957 (1984).

[10] J. E. Keem, J. M. Honig, and L. L. Van Zandt, Philos. Mag. B **37**, 537 (1978).

[11] F. P. Netzer and M. Prutton, J. Phys. C **8**, 2401 (1975); M. R. Welton-Cook and M. Prutton, *ibid.* **13**, 3993 (1980).

[12] C. G. Kinniburgh and J. A. Walker, Surf. Sci. **63**, 274 (1977).

[13] M. Yan *et al.*, Philos. Mag. A **72**, 121 (1995).

[14] Th. Bertrams *et al.*, Appl. Surf. Sci. **75**, 125 (1994).

[15] D. Adler, in *Solid State Physics*, edited by F. Seitz, D. Turnbull, and H. Ehrenreich (Academic, New York, 1968), Vol. 21, p. 1.

[16] J. Kübler and A.R. Williams, J. Magn. Magn. Mater. **54-57**, 603 (1986).

[17] A. Freitag *et al.*, Chem. Phys. Lett. **210**, 10 (1993).

[18] A. Gorschlüter and H. Merz, Phys. Rev. B **49**, 17 293 (1994).

[19] J. M. McKay and V. E. Henrich, Phys. Rev. B **32**, 6764 (1985).

[20] S. L. Dudarev, D. Nguyen Manh, and A. P. Sutton, Philos. Mag. B (to be published).

[21] L. F. Mattheiss, Phys. Rev. B **5**, 290 (1972).

[22] P. W. Anderson, in *Solid State Physics*, edited by F. Seitz and D. Turnbull (Academic, New York, 1963), Vol. 14, p. 99.